Food Research International 221 (2025) 117135

Contents lists available at ScienceDirect

Food Research International

journal homepage: www.elsevier.com/locate/foodres

In silico investigation of hydrodynamics of low viscosity liquids for INFOGEST gastric phase☆

Shaktivesh Shaktivesh [a], Matt D. Sinnott [a,*], Alan R. Mackie [b], Paul W. Cleary [a]

[a] Commonwealth Scientific and Industrial Research Organisation (CSIRO) Data61, Australia
[b] The School of Food Science and Nutrition, University of Leeds, Leeds LS2 9JT, UK

ARTICLE INFO

Keywords:
Semi-dynamic *in vitro* digestion model
INFOGEST protocol
Stirring
Fluid transport
Mixing
Smoothed particle hydrodynamics

ABSTRACT

The INFOGEST network has proposed standardised semi-dynamic *in vitro* models by expanding upon the INFOGEST static model protocol to incorporate the kinetics of the gastric phase. This includes gradual acidification, secretion of fluids and enzymes, gastric emptying, and stirring. Continuous stirring is expected to disperse added gastric fluids and enzymes for digestion while engaging the fluid in motion. How effectively advective mixing produced by the INFOGEST stirrer represents incomplete mixing of gastric fluid with food substrates *in vivo* is not yet understood. We present the first *in silico* prediction of hydrodynamics around the INFOGEST stirrer based on the Smoothed Particle Hydrodynamics (SPH) numerical method. This is used to investigate digesta circulation and dispersive transport of injected gastric fluid and enzymes across a range of viscosities that represent different stages of gastric digestion for a low viscosity Newtonian liquid food following a standardised semi-dynamic protocol. Three sets of conditions were considered corresponding to the start, one hour, and two hours into gastric digestion. Flow behaviour reveals strong azimuthal swirl, complex radial and axial recirculation and mixing. Transport is affected by viscosity and fill level. Higher viscosities (0.05 Pa.s) during the initial stage were found to hinder radial dispersion of gastric fluid and enzymes, potentially slowing early digestion. Fluid beneath the stirrer remains stagnant throughout all digestion stages, indicating denser digesta that settle to the bottom may remain undigested. The model predictions for gastric digesta mixing using the INFOGEST stirrer give encouraging evidence that, at least for simple liquid foods, the stirrer design can produce the extent of spatial variation in digesta composition and hydrolysis rates required by the semi-dynamic protocol and similar to the incomplete mixing observed *in vivo*.

1. Introduction

Food consumption significantly impacts human health, necessitating a deep understanding of how food is digested throughout the gastrointestinal tract to improve bioavailability. Many *in vitro* models have been developed to replicate physiological conditions and the sequence of digestive functions occurring in humans (Lucas-González et al., 2018). These models have evolved from simple static setups to more complex semi-dynamic and dynamic configurations. Static *in vitro* models are cost-effective, easy to set up, and benefit from internationally harmonised protocols established by the COST Action INFOGEST network, which minimise variability of the experimental conditions (Brodkorb et al., 2019). However, they do not replicate dynamic food digestion processes such as shearing and mixing caused by gut wall peristalsis nor the temporal changes that occur during digestion (Cardoso et al., 2015). Dynamic models are more physiologically relevant as they mimic the gradual passage of ingested food through the gastrointestinal tract using multicompartment setups and consider the dynamic nature of physiochemical conditions through computer-controlled systems. Nonetheless, such *in vitro* models have had limited application due to their complexity, expense, and lack of standardised validation protocols (Alminger et al., 2014).

Recognising the limitations of existing static and dynamic *in vitro* digestion models, efforts have focused on developing semi-dynamic *in vitro* models that strike a balance between the dynamic nature of the digestion process and experimental feasibility. As a compromise, Mulet-Cabero et al. (2020) proposed a standardised protocol for semi-dynamic *in vitro* models based on the INFOGEST static *in vitro* food digestion

☆ This article is part of a Special issue entitled: 'ICFD2024' published in Food Research International.

* Corresponding author.
E-mail address: matthew.sinnott@csiro.au (M.D. Sinnott).

https://doi.org/10.1016/j.foodres.2025.117135
Received 30 October 2024; Received in revised form 3 May 2025; Accepted 26 July 2025
Available online 29 July 2025

protocol (Brodkorb et al., 2019). This incorporates dynamic gastric and static intestinal phases. During the dynamic gastric phase, gastric fluid and enzymes are gradually added to a vessel holding gastric digesta. The mixture is continuously stirred at 10–15 rpm using an overhead stirrer. Periodic samples are taken from the vessel using aliquots to mimic gastric emptying, with each sample used for the subsequent static intestinal phase models. While this stirring does not necessarily replicate *in vivo* mechanical forces, it aids in the mixing of gastric digesta which promotes interactions between enzymes and food components.

According to the semi-dynamic INFOGEST protocol guidelines, using a V-form (titration) vessel and maintaining a low speed between 10 and 15 rpm is recommended to achieve partial mixing, emulating the *in vivo* scenario for weak mixing and minimal agitation in the fundus and body of the stomach. This model is unable to represent the mechanical forces in the antrum responsible for motility, stronger mixing and phase separation (creaming, sedimentation and gastric sieving). How much of the digesta volume is mobilised by the stirrer (to represent antral recirculation) and the size and extent of unmixed regions (to represent incomplete mixing in the upper stomach) has not yet been well characterised. The presence of stagnant flow regions hinders the completeness of mixing of gastric fluid and enzymes throughout the digesta, which in turn can affect enzyme function, limiting interaction between food components and enzymes, and altering digestion kinetics. As such, the rate of digestion may be poorly estimated, potentially leading to underestimation or overestimation of food breakdown (Bornhorst, 2017). Given that the physical properties of digesta, such as viscosity, change during gastric digestion (Jin et al., 2023; Logan et al., 2014), a critical question arises: How effectively does a constant speed overhead stirrer mix the digesta and disperse the added gastric fluid and enzymes? Understanding this is important for understanding digestion kinetics and any differences between the different intestinal (well mixed) digestions applied to the different gastric emptying events. Investigating the transport of enzymes and acids in *in vitro* models presents challenges, particularly in tracing their dispersion in three-dimensional space since the stirrer at least partially obscures visibility.

Computational Fluid Dynamics methods, either grid-based or meshfree/particle-based, offer a powerful alternative for studying these problems. Numerical simulation of digesta stirring includes prediction of the fluid free surface and the interaction with the stirrer. Since the digesta is stirred gently at low speed, the free surface deformations are not large compared to vigorous stirring and can be simulated using either type of method. A grid-based method needs a complex mesh around the surface of stirrer that must either rotate (using a slip mesh approach) or adapt continuously with the stirrer rotation. Conversely, a Lagrangian approach such as Smoothed Particle Hydrodynamics (SPH) uses numerical "particles" to represent equipment surfaces and the freely moving fluid which being unstructured easily conforms to the stirrer surface without special numerical treatments. SPH also mitigates issues relating to advection causing numerical diffusion near sharp discontinuities in fluid properties, (which can be more challenging for grid-based or Eulerian methods). When tracking mixing of materials, particularly multiple materials with complex interfaces, the use of such a particle method for fluid mixing simulations can be beneficial (Cleary et al., 2007). Although grid-based methods can simulate the fluid flow problem in this study, SPH handles it with ease and accuracy. The future potential in modelling digestive systems using multi-physics particle methods is in its natural representation of more realistic complex food materials and multiphase flows, especially for direct prediction of spatial and temporal rheological change from first principles based on local solids fraction.

Existing studies related to gastric digestion have primarily concentrated on the dynamics of mixing, flow characteristics, and multiphase environments within the stomach (Ferrua et al., 2014; Harrison et al., 2018; Li & Jin, 2023; Liu et al., 2023). Despite the widespread use of *in vitro* models in gastric digestion studies, such as semi-dynamic models, there remains a paucity of studies employing fluid dynamic simulations to address issues relevant to *in vitro* gastric digestion.

In this study, we develop an *in silico* model of a semi-dynamic INFOGEST gastric phase protocol for digestion of a simple low viscosity Newtonian liquid as a first model food. This study is the first model prediction of hydrodynamic performance for the INFOGEST stirrer. It uses SPH simulation to predict digesta flow and dispersion of injected gastric fluid in a titration vessel by an overhead stirrer during different stages of gastric digestion of liquid food. Such insights can then be used to inform *in vitro* equipment selection, design and choice of experimental parameters for more physiological representation of the digestion process.

2. Numerical method: Smoothed particle hydrodynamics (SPH)

Simulating hydrodynamics generated by agitation in a semi-dynamic *in vitro* model poses challenges due to the geometry of the INFOGEST stirrer, the dynamic interactions between fluid and vessel, and between fluid and stirrer, and the changing free surface. To effectively simulate such an environment, a robust and accurate computational fluid dynamics (CFD) method is needed. The SPH methodology is well published (Monaghan, 2005; Cleary et al., 2007, 2021; Sinnott et al., 2021). For examples of application to biophysical and complex industrial flow applications see Cleary et al. (2007, 2021). SPH has also previously been used to simulate flow and mixing in a closed helical mixer device which although on a larger scale is quite similar to the mixing in the INFOGEST stirrer (Robinson & Cleary, 2012).

The SPH code used in this paper has been previously validated on a broad range of flow problems such as suspension of cylindrical wood pellets in a mixing tank filled with water (Prakash et al., 2007), impact loading time history of interaction between dam-break flow and rectangular column located downstream (Cummins et al., 2012), water filling in die of laptop computer chassis (Cleary et al., 2014), and other casting flow processes (Cleary et al., 2002).

3. INFOGEST gastric phase protocol

As per the semi-dynamic INFOGEST protocol, the gastric phase of the *in vitro* geometry involves several components, including a titration vessel and overhead stirrer (Mulet-Cabero et al., 2020) which are shown diagrammatically in Fig. 1. Simulated digestive juices and enzymes are continuously and independently delivered through separate tubes into the resident digesta within the vessel. To reduce obstruction of the digesta flow field (and subsequent mixing), these tubes are usually positioned near the vessel wall with the tube outlet ends as close to the bottom of the vessel as possible. The resident digesta and introduced fluids undergo continual mixing using an INFOGEST standard overhead stirrer with a rotational speed in the range, 10–15 rpm (as detailed in the supplementary material of Mulet-Cabero et al. (2020) and shown in Fig. 1). Emptying is performed in a stepwise manner by manually taking the selected aliquots at calculated times from the bottom of the vessel using a laboratory tool with an end diameter of ~3 mm. Actual aliquot sample volume depends on the planned number of emptying times and the initial gastric volume.

3.1. Simulation setup

A critical issue for modelling this system is that of disparate timescales. The fluid dynamic timescale is short (order seconds) while the digestion timescale is of the order of hours. Direct calculation of the fluid dynamics over the full digestion timescale is both impractical and unnecessary. The effect of the progressive digestion is to change the general conditions of the fluid in the mixer. This digesta change and accompanying operating condition changes (such as fill level) are explicitly catered for by performing simulations at three different times (and therefore different stages of the digesta evolution). Each simulation is performed for a sufficiently long time to establish the nature of the

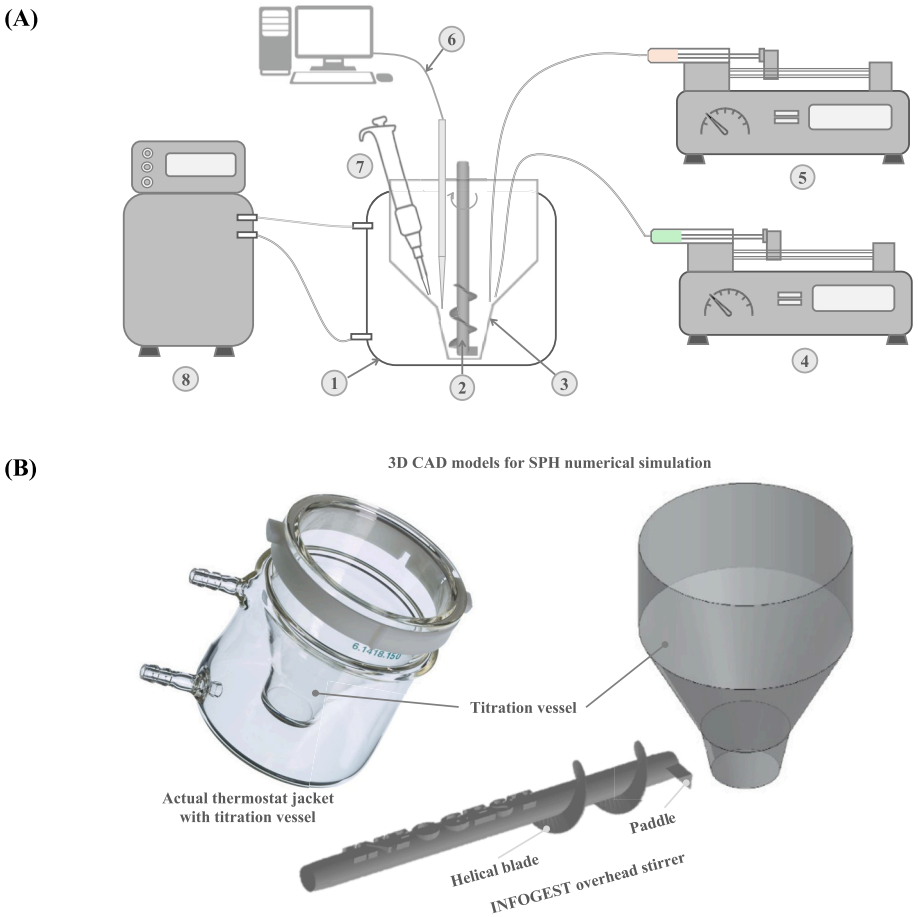

Fig. 1. (A) Schematic diagram of Gastric phase of INFOGEST Semi-Dynamic *In Vitro* Model, (1) Thermostat jacket (2) INFOGEST overhead stirrer, (3) Titration Vessel, (4) Electrolyte Simulated Gastric Fluid (eSGF) and HCl Pump, (5) Enzymes secretion solution (pepsin and gastric lipase) pump, (6) pH probe, (7) Aliquot for gastric emptying, (8) Water bath circulator; (B) 3D CAD models of Titration vessel (5–70 mL) and INFOGEST overhead stirrer (composed of helical blade wrapped around the cylindrical rod, and wedge-shape paddle attach at the end of cylindrical rod of stirrer), built for SPH numerical simulation.

fluid dynamics (the fluid dynamic timescale) and therefore mixing at that set of digestion conditions.

Logan et al. (2014) has reported viscosities of 0.050, 0.010, and 0.007 Pa.s respectively for a representative liquid food (orange juice solution) at the start (labelled as t_0), after one hour (labelled as t_1), and two hours (labelled as t_2) into gastric digestion process. These viscosities are used for the SPH simulations representing the different stages of digestion corresponding to t_0 (0 h), t_1 (1 h), and t_2 (2 h) The density of the digesta is 1 g/cm^3. Table 1 summarises the details for each simulation.

Table 1
Summary of the *in vitro* experiment conditions used for each simulated gastric stage (representing time points t_0, t_1 and t_2).

Time points (hr)	Vessel content	Apparent viscosity (Pa·s)	Total volume added in vessel from start (mL)	Total gastric emptied volume (mL)	Net volume in the vessel (mL)
0 (t_0)	Oral bolus + basal volume	0.050 (η_0)	25.30	0.0	25.30
1 (t_1)	Oral bolus + basal volume + simulated gastric fluid + enzyme	0.010 (η_1)	31.48	1 × 9.2 = 9.2	22.28
2 (t_2)	Oral bolus + basal volume + simulated gastric fluid + enzyme	0.007 (η_2)	37.66	3 × 9.2 = 27.6	10.06

The amount of fluid in the mixing vessel is varied according to the semi-dynamic INFOGEST protocol due to both addition of new fluids and sampling removal of existing fluids (Mulet-Cabero et al., 2020). During the gastric phase, artificially prepared gastric fluid, referred to as simulated gastric fluid (SGF) in the *in vitro* protocol is continuously added to the digesta in the vessel. The SGF solution represents *in vivo* gastric secretions and consists of electrolyte simulated gastric mixture, enzymes, HCl, Ca^{2+} solution, and water. Using an initial liquid food sample size of 20 mL all other volumes can be calculated as outlined below.

At the start of the gastric phase (simulation performed at t_0), the vessel initially contains a fluid volume of 25.3 mL. This comprises 23 mL from the oral phase (20 mL of food volume and 3 mL of simulated salivary fluid) and a gastric basal volume containing 10 % of the SGF, which is 2.3 mL. The remaining 90 % of the SGF (minus enzymes) and 90 % of the remaining enzyme mixture are gradually introduced into the vessel through two tubes at rates of 0.093 mL/min and 0.010 mL/min. These rates of addition are used to calculate the total fluid volume that is added at t_1, and t_2 and used for the matching SPH simulations for the later stages of digestion. Additionally, periodic gastric emptying events remove 9.2 mL of digesta every 40 mins. So,

- for gastric stage (t_1), the net fluid volume is 25.3 + (0.093 mL/min × 60 mins) + (0.010 mL/min × 60 mins) − 9.2 mL = 22.28 mL.

- for gastric stage t_2, which follows three gastric emptying events, the net volume is reduced to only 10.06 mL.

The added gastric fluid and enzymes are assumed to have the same viscosity and density as the original fluid.

3D CAD geometries for the INFOGEST stirrer and titration vessel were constructed and pre-processed as SPH objects. The stirrer design is available in the supplementary material for the semi-dynamic INFOGEST protocol (Mulet-Cabero et al., 2020). It consists of a central shaft, a helical blade and a wedge-shaped paddle at the bottom (see Fig. 1B for details). The titration vessel (Metrohm order no. 6.1418.150) has a double-conical shape with the upper conical section having a larger cone angle than the lower section. The pre- and post-processing is done using CSIRO Workspace (Workspace, 2024; Cleary et al., 2020) which is used to combine and automate operations into scientific workflows.

For each gastric stage simulation, the vessel is initially filled to the desired fill level and allowed to settle before the stirrer rotation is initiated to give a quiescent initial state. A resolution of 0.25 mm is used for fluid and boundary discretisation giving fluid particle numbers of 2.02 million, 1.83 million and 1.04 million for t_0, t_1, t_2 respectively. The stirrer has a constant rotation speed of 15 rpm for all gastric stages.

To investigate how specific transport characteristics might influence the rate and extent of digestion at each gastric stage, we track fluid initially within two regions of interest (ROI):

1) ROI1 defines the fluid sub-volume around the feed tubes where model gastric secretions (SGF, acid and enzymes) are introduced to the titration vessel. It is located near the bottom and adjacent to the vessel walls (see Fig. 2). Since dispersion of the secretions is not instantaneous nor necessarily homogeneous, the degree to which these mix with the resident digesta will influence acid/enzyme availability for further digestion of the model food.
2) ROI2 defines the basal region beneath the stirrer, between the underside of the stirrer and the vessel floor, where denser components of food and digesta may settle.

3.2. Mixing measure to track fluid dispersion

Mixing of a discrete fluid sub-volume (*e.g.* containing high concentration of added acid and enzymes) can be characterised by tracking the centroid for this group of fluid particles over time (Harrison et al., 2018). As the sub-volume disperses radially, azimuthally and axially throughout the total resident fluid in the vessel, the distance of each centroid component from the overall fluid centre of mass is a measure of the degree of radial and axial mixing respectively. Note that mixing can be quite anisotropic and can be quite different for each direction. The rate of mixing for each centroid component can often be determined by fitting an exponentially declining sinusoidal function, where the oscillation is related to the periodic stirring process and the nature of the flow field that arises from it.

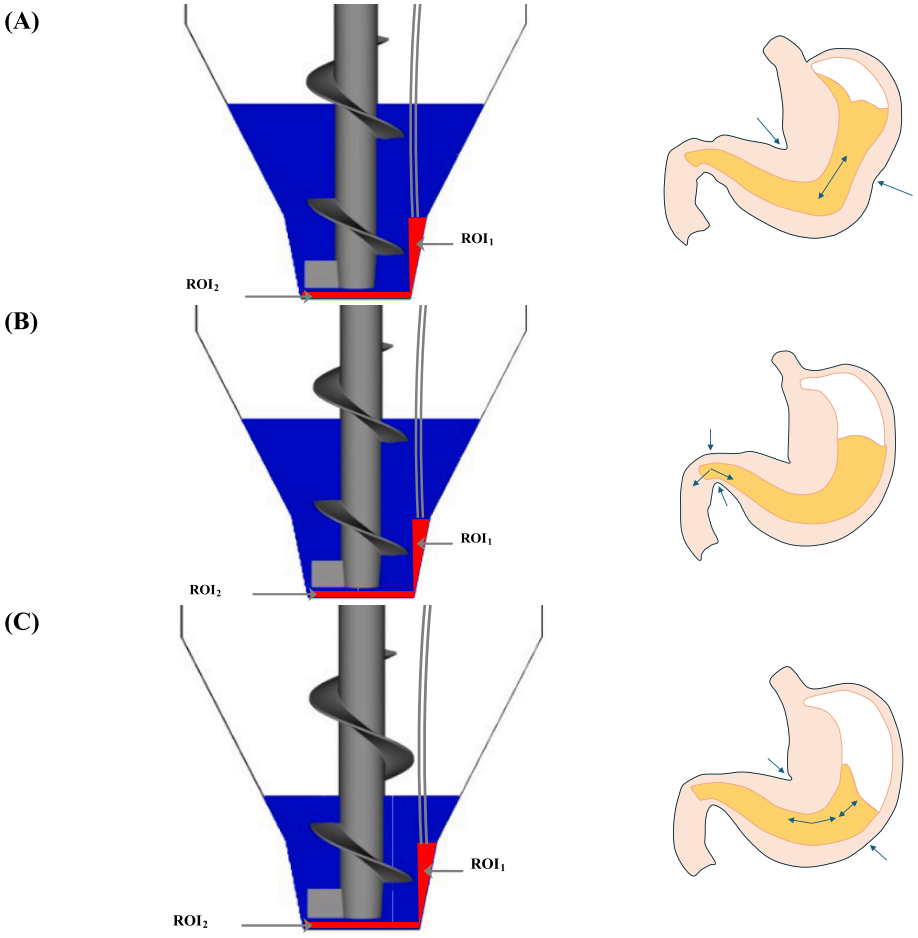

Fig. 2. Schematic diagram of each gastric stage batch simulation (A) 0 h (t_0), (B) 1 h (t_1) and (C) 2 h (t_2) containing fluid digesta, stirrer and vessel. The highlighted red regions of interest for the dispersion analysis are ROI1 (corresponding to where SGF, acid and enzymes are introduced in *in vitro* experiments) and ROI2 (the basal region underneath the stirrer). On the right are conceptual images of representative *in vivo* gastric states corresponding to each of the *in vitro* stages. The arrows indicate peristaltic wall contraction and fluid flow towards the pylorus. This is intended to highlight low peristaltic activity in the fundus region as well as emptying of the gastric fluid volume throughout the INFOGEST protocol. (For interpretation of the references to colour in this figure legend, the reader is referred to the web version of this article.)

4. Fluid transport characteristics

Each gastric stage simulation is run until quasi-steady periodic flow is fully established. The time taken for initial flow transients to dissipate is 0.35 s for t_0, 0.6 s for t_1 and 0.45 s for t_2. This follows sensible trends with viscous dissipation and fluid volume. Fig. 3 shows the fluid flow represented by a velocity arrow field in a mid-section (X-Z) plane through the centre of the titration vessel for each simulation. The stirrer rotates clockwise and the data for each gastric stage is shown at the same phase of stirrer motion for ease of comparison. The velocity arrows are coloured and scaled in length by local fluid speed.

The rotating stirrer imparts a dominant swirling motion to the fluid in the azimuthal direction. Superimposed over this motion are strong radial/axial circulation regions around the blade tip in the upper conical section where there is sufficient distance between the blade tip and wall. Here, fluid underneath the blade is directed downward along the shaft and radially outward by the descending blade, which then flows up around the blade tip and radially back inward towards the shaft. For fluid much closer to the stirrer shaft, there is a strong vertically downward axial flow felt all the way along the length of the shaft to the upper surface of the next helical turn. In the lower conical section, the circulation regions greatly diminish due to the much smaller gap between blade tip and the axial component of flow under the blade is almost predominantly directed downward. Fluid immediately above the paddle, is pushed very strongly upward by the inclined leading face of the wedge shape which pushes into the swirling flow.

When the fluid free surface is in the upper conical section of the titration vessel for simulations t_0 and t_1, fluid adjacent to the vessel wall in the upper section is largely stagnant. In contrast for t_2 where the much smaller volume of fluid mainly occupies the lower conical section, the

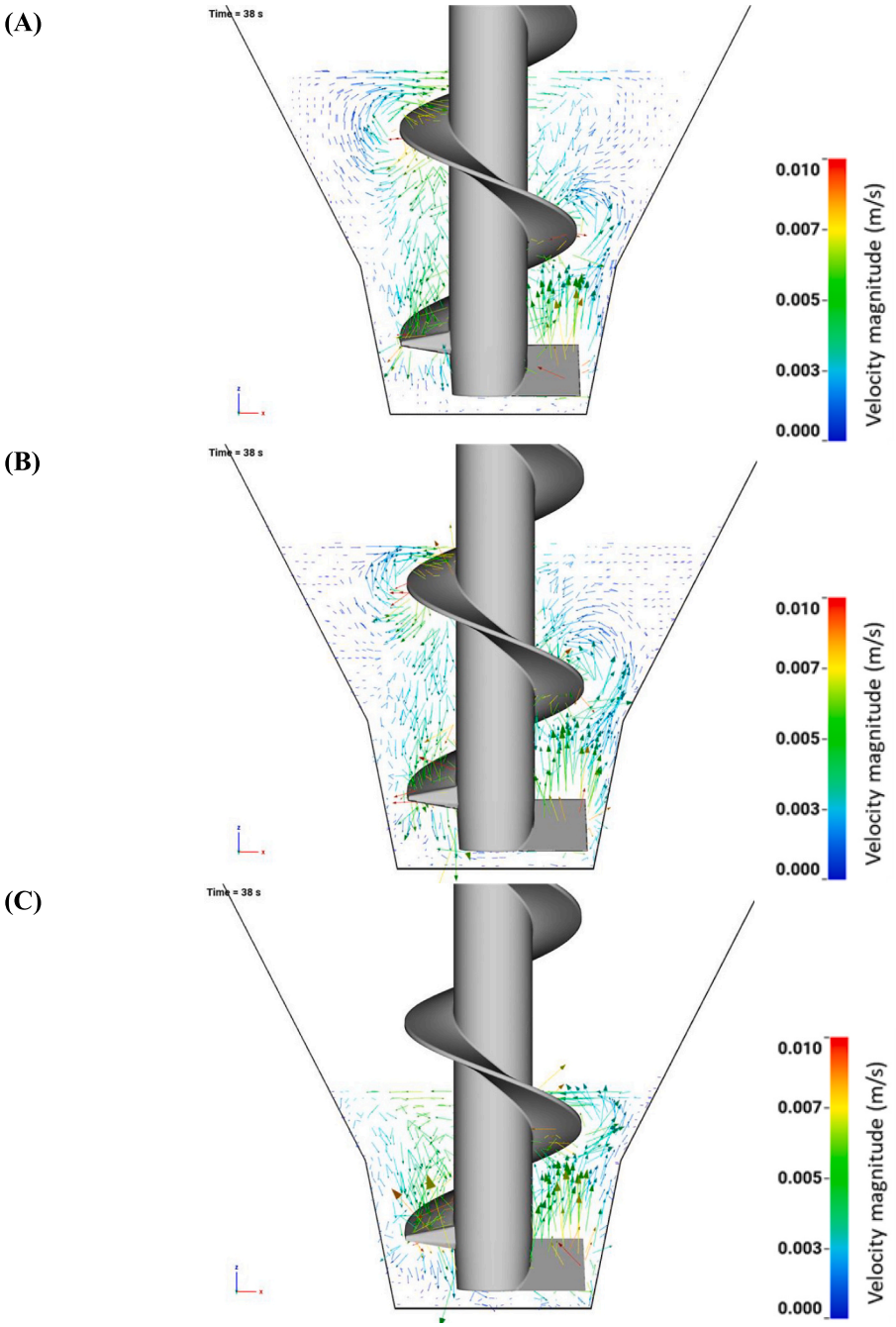

Fig. 3. Flow field represented by velocity vector arrows at time (A) 0 h (t_0); (B) 1 h (t_1); (C) 2 h (t_2). Velocity vectors are coloured and scaled in length by fluid speed.

much smaller gap between blade tip and vessel wall and the reduced viscosity results in greater mobility of most of the fluid volume.

Fig. 4 shows the principal components of fluid velocity in the same mid-section (X-Z) plane for each gastric stage simulation. The rows show the flow coloured by speed, axial (V_z), azimuthal (V_t), and radial (V_r) velocities. Columns correspond to the simulations.

For t_0, the fluid speed (Fig. 4, row 1) shows that the peak fluid speeds (red) are highly localised around the tips of the blade and immediately above the paddle. The dark blue areas indicate slow flow or stagnation below the stirrer and out towards the walls, particularly in the upper conical section of the vessel. The axial speed (Fig. 4, row 2) shows that the helical blade motion produces a moderate and steady bulk flow

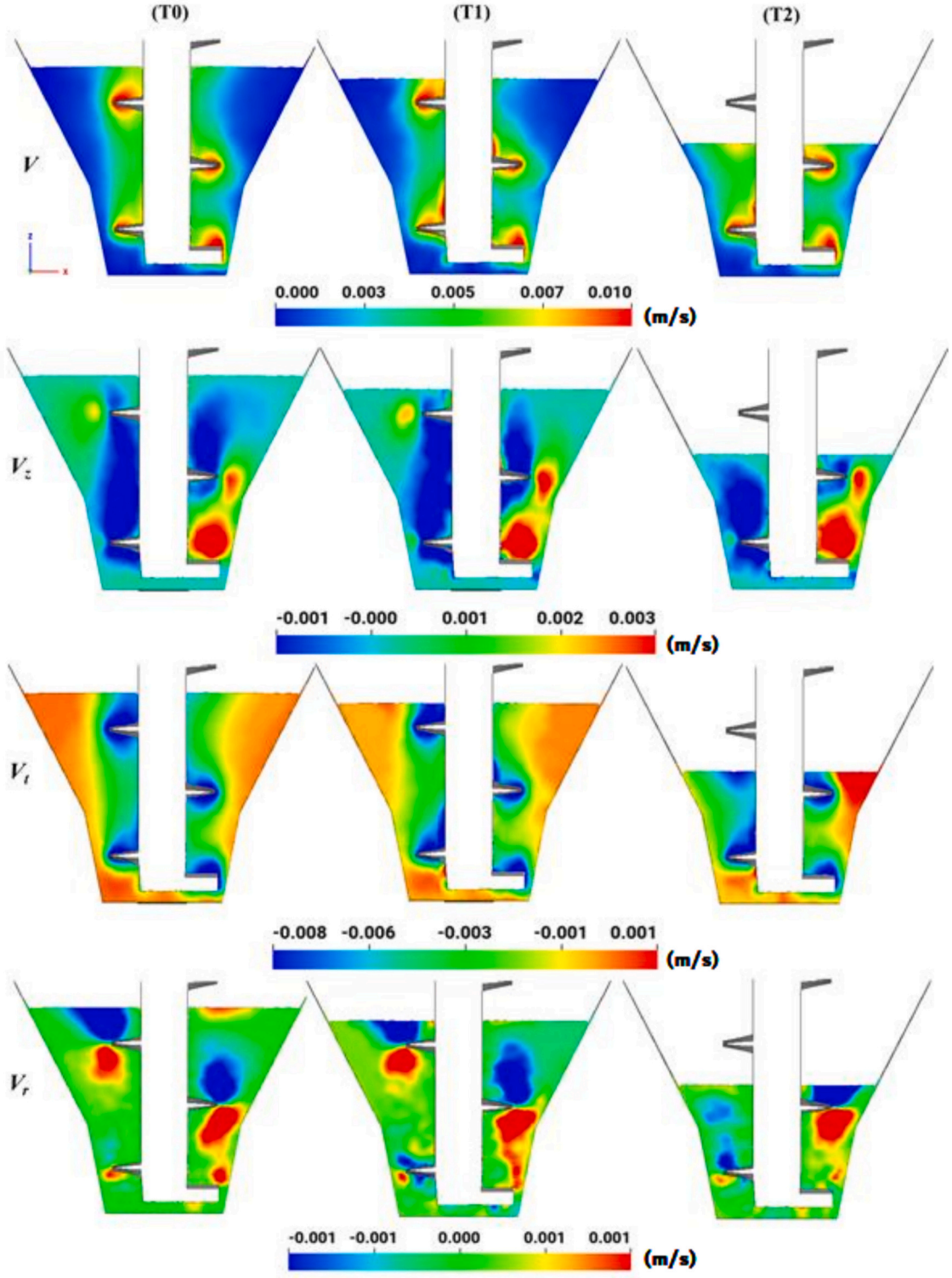

Fig. 4. Digesta flow in a vertical mid-plane. The flow is represented by colour flooded plots showing: [Row 1] total fluid speed (V); [Row 2] axial speed (V_z); [Row 3] tangential speed (V_t); and [Row 4] radial speed (V_r), all with units of m/s. Column (A) is the gastric stage at 0 h (t_0), column (B) is at 1 h (t_1), and column (C) is at 2 h (t_2).

down around the impeller shaft within a cylindrical envelope near the edges of the stirrer blade. On the side of the stirrer containing the paddle, there is also a strong upward directed flow extending upwards to two-thirds of the vessel height and which spreads out and around the helical blade above. The opposing flows induced by blade and paddle produce strong vertical circulation that is important for axial transport and mixing (as well as transporting introduced SGF to digesta into the upper half of the titration vessel). The azimuthal velocity (Fig. 4, row 3) shows the nature of the swirling flow created by and around the stirrer. Fluid near the blade is entrained at around 70 % of the tip speed. Moderate swirl (with speeds around 20 % of tip speed and coloured green) is present in a long cylindrical region that encompasses most of the length of the impeller and extends a short distance radially beyond the blade tips. The swirl rapidly decreases with radial position beyond this, so that there is very little azimuthal transport in the upper outer parts of the vessel (coloured orange). For the radial speed (Fig. 4, row 4), fluid underneath the blade tends to be pushed radially outward, while fluid above the blade flows inward. This radial circulation around the blade tip becomes substantially weaker in the lower conical section where the blade/wall gap is smaller. The radial and axial flow components combine to produce the circulation structures around the blade tips previously identified in Fig. 3.

For the gastric stage t_1, a strong reduction in viscosity by 80 % and a mild reduction in fill volume of 12 % together result in only modest changes to the flow behaviour. Specifically, the cylindrical envelope of the high swirl core of the flow which now contacts the wall in the lower conical section becomes significantly distorted. Radial circulation around the blade tip increases in intensity in the lower half of the vessel. Elsewhere, radial and angular velocity structures mildly change in minor details but without notable transport consequences.

After two hours of gastric digestion (t_2), the reduction of 60 % in fill volume and 30 % in viscosity creates more dramatic change in flow behaviour. There is greater mobility of almost the entire fluid volume. Axial transport significantly increases with upward flow from the paddle extending all the way to the free surface. The high swirl core also fully extends to the wall at all heights so that there is a large reduction in the volume of stagnant or slow flow. The only remaining such regions are thin wall boundary layers and a small region between the bottom corner

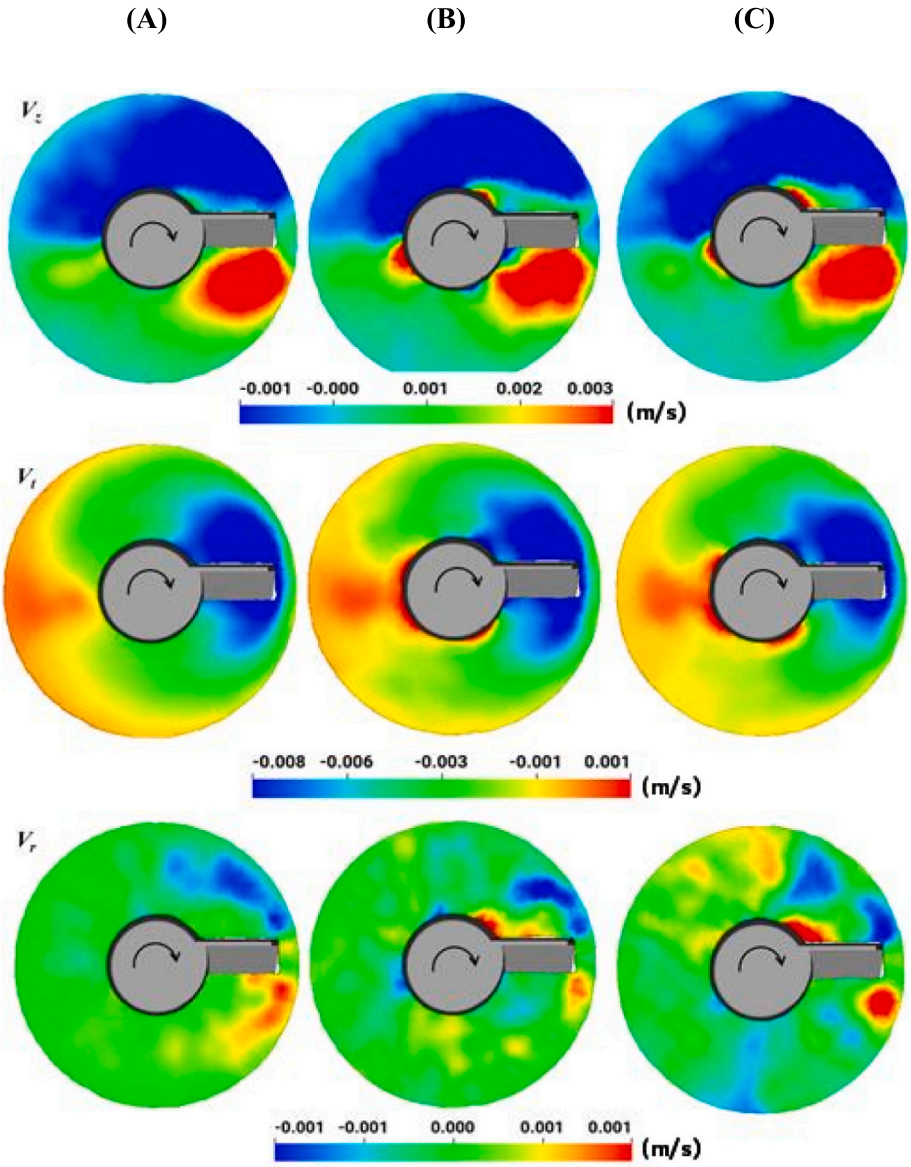

Fig. 5. Digesta flow in an axial slice showing the effect of the paddle on the flow. The slice is located at the mid-height of the stirrer paddle. Flow is represented by colour flooded plots showing: [Row 1] axial speed (V_z); [Row 2] tangential speed (V_t); and [Row 3] radial speed (V_r), all with units of m/s. Column (A) is the gastric stage at 0 h (t_0), column (B) is at 1 h (t_1), and column (C) is at 2 h (t_2).

of the vessel and the bottom turn of the helical blade. The change in fill level appears to be the dominant influence on flow behaviour for the latter digestion stage.

Fig. 5 shows the effect of the paddle on the flow in a horizontal axial slice (X-Y plane), located at the mid-height of the paddle. The top row shows the flow field represented as velocity vectors with latter rows showing the flow coloured by speed, axial (V_z), azimuthal (V_t), and radial (V_r) velocities. The columns again represent each gastric stage.

For t_0, the primary role of the scooping action of the paddle is seen to be the generation of vertical transport which is a critical aspect of mixing. There is stronger upward flow concentrated in a 45-degree sector immediately in front of the paddle mid-section as fluid is forced upward by the inclined leading face of the paddle. Steady downward directed return flow is visible within a 180-degree azimuthal sector trailing the paddle. The rotating paddle generates strong azimuthal swirl throughout much of this level of the vessel (Fig. 5, row 2). There is mild radial motion in the quadrants in front of and behind the paddle (Fig. 5, row 3). Such radial transport is important for effective mixing so the limited region in which the radial velocities are high means that mixing is restricted. For the other gastric stages t_1 and t_2, the vertical motion generated by the paddle is broadly similar.

Fig. 6 shows the effect of the helical blade on the flow in an axial slice (X-Y plane) at the same instant (and stirrer phase) as Fig. 5. The slice is located at 16.5 mm from the vessel bottom which is just inside the upper conical section of the vessel. The top row shows the flow field represented as velocity vectors with rows showing the flow coloured by speed, axial (Vz), azimuthal (Vt), and radial (Vr) velocities respectively. The columns represent gastric stages.

For gastric stage t_0, the rotating blade produces downward transport (coloured dark blue) in the elliptical shape surrounding the impeller. It is asymmetric with the downward flow only extending forward a short distance in front of the blade but a large distance behind – reaching the wall of the vessel. A strong balancing upward flow (coloured red) occurs in a long arc shaped region adjacent to the vessel wall starting at the blade and extending clockwise around the vessel. This upflow starts at the bottom paddle which is located directly beneath. Much of the fluid in this cross-section rotates along with the rotation of the impeller but with magnitude decreasing with distance. Fluid coloured green swirls at a

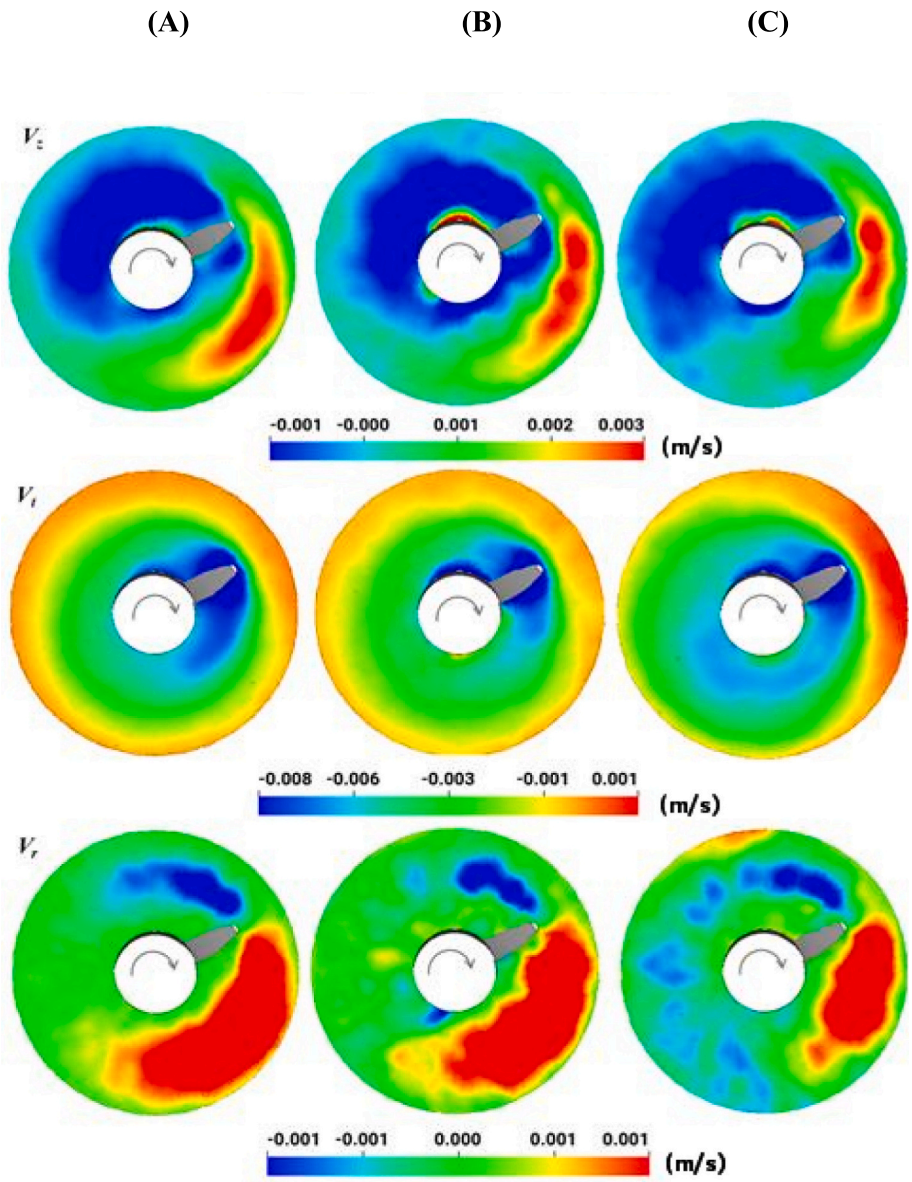

Fig. 6. Digesta flow in an axial slice showing the effect of the helical blade on the flow. The slice is located at 16.5 mm from the bottom of the vessel. Flow is represented by colour flooded plots showing: [Row 1] axial speed (V_z); [Row 2] tangential speed (V_t); and [Row 3] radial speed (V_r), all with units of m/s. Column (A) is the gastric stage at 0 h (t_0), column (B) is at 1 h (t_1), and column (C) is at 2 h (t_2).

reasonable rate and occupies an elliptical region that extends just beyond the blade and decreases to zero at the vessel wall. The peak tangential speeds (dark blue) imparted by the blade occur within a compact circular region around the blade which connects to a band of strong swirling flow in advance of the blade. The passage of the blade creates significant radial transport with flow directed radially outward (coloured red) in advance of the blade with a weaker inward return flow behind the blade. The rotating impeller generates a strong coherent flow pattern which will stretch the fluid out, but this does not necessarily produce the folding action that is needed for effective mixing.

The region of strong outward radial motion ahead of the blade for t_2 decreases strongly whilst the area of inward flow (light and dark blue) now extends over a significant fraction of the perimeter of the vessel. The structure of the radial motion is less coherent for the reduced viscosities the emergence of finer scale structure which is likely to be at least mildly positive for mixing.

Poorly mixed regions can be well identified using fluid shear rate (which is proportional to the 2nd invariant of the strain rate tensor of the flow field). This is done by averaging the SPH velocities onto an Eulerian grid which is used to calculate the strain rate tensor at each grid point. The shear rate represents the rate of deformation of the digesta. Fig. 7 shows the spatial distribution of shear rate in the same vertical slice used in Fig. 4 for each gastric stage. For t_0 (Fig. 7A) the dark blue regions in the upper corners of the vessel, and below the stirrer extending out to the bottom right-hand corner opposite the paddle have low shear rates ($<$ 0.1 1/s). The fluid transported within the stirrer has moderate shear rates of ~1 (1/s) across the full height of the fluid volume. The outer edge of the paddle and the screw generate peak shear rates of 3 (1/s) which arise from the radial circulation zones identified in Fig. 4. The average shear rate of 0.25 (1/s) is roughly constant with height and is consistent with physiological estimates of *in vivo* gastric shear rate (Li & Kong, 2022). With the five-fold reduction in viscosity at t_1, the shear rate distribution is less uniform with height inside the impeller and the zones of high shear rate shrink in size. The poorly mixed low shear rate regions persist. At the final gastric stage t_2, regions of peak shear rate at the edges of the impeller blade increase in intensity. Almost all low shear regions disappear except for the lower corner of the vessel opposite the paddle. This suggests that most of the fluid volume in the latter stages of the gastric phase is reasonably mixed.

The presence of significant stagnant fluid regions for t_0 and t_1 suggests that inadequate mixing (with poor delivery of SGF into these regions) may delay and/or limit the extent of digestion during the early stages of gastric stages as intended for the *in vitro* model.

5. Digesta mixing of select ROI regions

5.1. Dispersion and mixing of added gastric secretions

ROI_1 represents the region where model gastric secretions (SGF/acid and enzyme mixtures) are continuously added throughout the *in vitro* experiment. This is positioned near the vessel walls and in proximity to the paddle (as shown in Fig. 2). The flow field generated by the rotating stirrer has a complex structure and rotates with the stirrer as discussed in the preceding section. It is important to understand how and to what degree this added material is mixed with the fluid initially filling the vessel for each stage of gastric digestion. SPH particles that are initially contained within ROI1 are tagged and monitored to see how they disperse. This is well suited to a Lagrangian particle method. Understanding the nature of gastric fluid dispersion throughout the gastric phase is important for understanding transport related bias of digestion kinetics in the *in vitro* model and predictions of bioaccessibility.

The top row in Figs. 8 and 9, show the dispersed tagged fluid particles (initially within ROI1) which are coloured red for each of the three gastric stages. The bottom row shows the centroid of the tagged particles with radial position in Fig. 8 and axial position in Fig. 9. For comparison between t_0, t_1, and t_2, the radial and axial centroid positions are

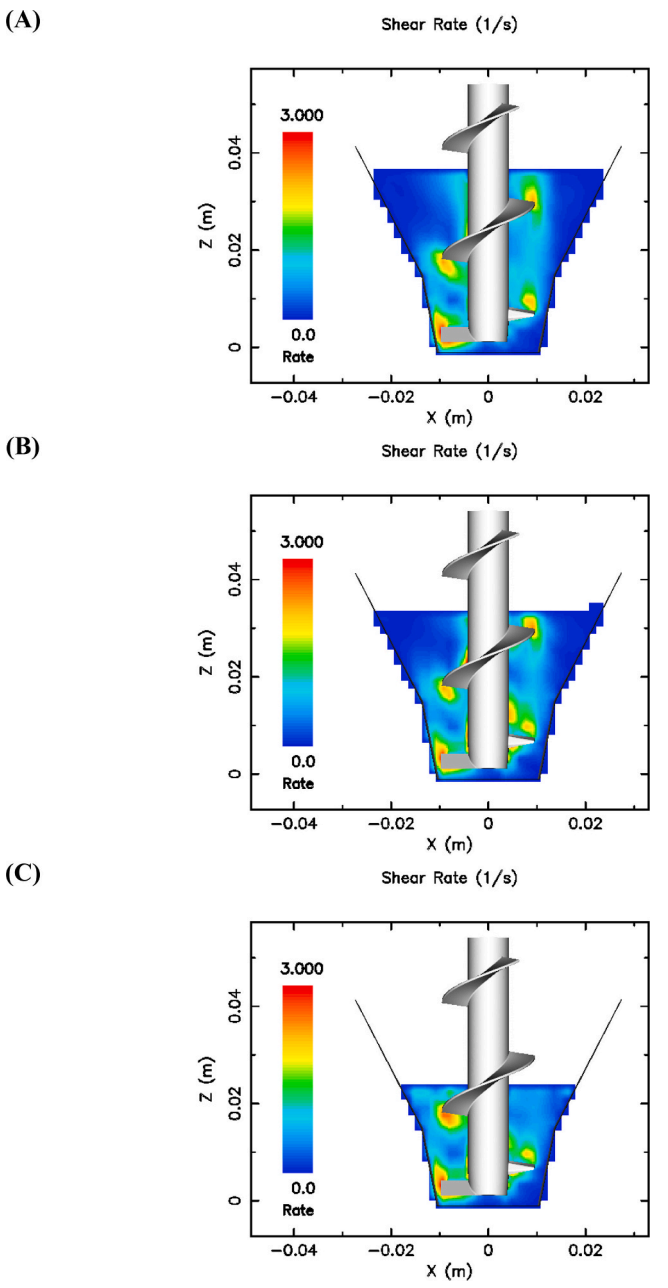

Fig. 7. Shear rate within the digesta produced by the mixing motion of the stirrer and shown in a vertical mid-plane for each gastric stage simulation: (A) t_0, (B) t_1 and (C) t_2. Regions of large shear deformation of the digesta fluid (yellow/red) and of stagnant poorly mixed regions (dark blue) are visible. (For interpretation of the references to colour in this figure legend, the reader is referred to the web version of this article.)

nondimensionalised by the stirrer radius and by the fill height above the ROI1 axial centroid position respectively. For gastric stage t_0, the red fluid is entrained by the fluid rotating with the stirrer, creating a coherent structure at a radius within the low-shear region between the stirrer and vessel wall, which leads to slow mixing. Conversely, for t_2, there is robust transport in both radial and axial directions indicating improved mixing.

Fig. 8D shows that the radial dispersion of added enzymes/acid is poor during the high viscosity, early gastric stage t_0. The radial centroid plateaus at 0.9 indicating a highly unmixed state. For t_1, the radial centroid steadily decreases to 0.45 over 40 s indicating significantly better radial mixing than occurs for t_0. The average radial dispersion rate

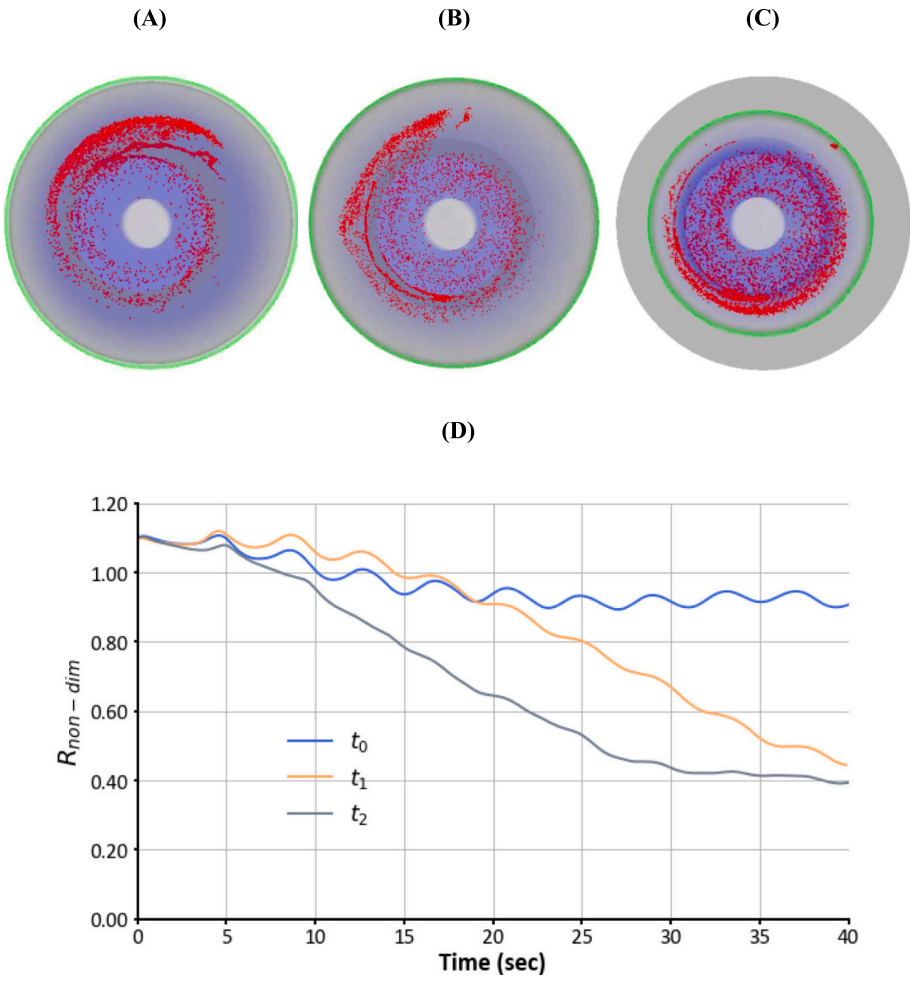

Fig. 8. Top view of the spatial dispersion of SGF injected into the lower corner of the vessel (region ROI1) (coloured red) at 40 s after the start of each gastric stage (A) t_0, (B) t_1 and (C) t_2. The green circles indicate the outer edge of the top (free) surface of the digesta. (D) Radial dispersion of the SGF as represented by the normalised radial centroid ($R_{non\text{-}dim}$) of the SGF particles for each gastric stage. (For interpretation of the references to colour in this figure legend, the reader is referred to the web version of this article.)

is 0.061 mm/s (t_0), 0.13 mm/s (t_1) and 0.19 mm/s (t_2). This suggests that digesta viscosity (which is 80 % lower than for t_0) is an important control for how well added enzymes/acid disperse within the titration vessel and that for high viscosity content mixing may be incomplete, hindering bioaccessibility. The latter gastric stage (t_2) which has a smaller fill volume and lower viscosity has much faster radial dispersion with an exponential decrease with time which plateaus at 0.4 by 30 s.

Fig. 9D shows substantial axial dispersion for all gastric stages. For t_0 and t_1, the strong axial recirculation discussed in Section 4 steadily transports the added enzymes/acid into the upper half of the vessel. The average axial dispersion rate is 0.5 mm/s (t_0), 0.6 mm/s (t_1) and 0.72 mm/s (t_2). There is only a weak dependence of the axial mixing on viscosity such that axial dispersion is around 20 % faster for t_1 than for t_0. Axial mixing is much faster in stage t_2 due to the shorter time required to traverse the smaller fluid depth.

5.2. Mixing in the basal region under the stirrer

Particles which are initially in ROI2, at the base of the vessel below the bottom of the stirrer, are also tagged and followed. The intent is to use the model to understand the degree to which the fluid (and implicitly any solids that may have settled to this region) are mixed back into the main fluid mass in order to allow this material to participate fully in digestive activity. Here we are only interested in vertical transport from this region.

The top row in Fig. 10, shows dispersion of the tagged fluid particles associated with ROI_2 (which are coloured red) for t_0, t_1, and t_2. The bottom row shows the change in the axial centroid of the tagged fluid particles. For comparison between stages, the axial positions of the centroid of ROI_2 are again nondimensionalised by the difference between ROI axial centroid position and the fluid height used in each gastric stage.

The fluid beneath the paddle is predominantly stagnant. The recirculatory flow in front of and behind the paddle mixes the fluid at the level of the paddle and above, but this does not extend much below the bottom of the paddle leaving most of this fluid stagnant. Consequently, the fluid beneath the stirrer (ROI_2) remains largely unmixed throughout all three digestion stages. A small amount of red material is entrained by the paddle and pulled upwards (Fig. 10A-C). Fig. 10D shows that mixing rate is very slow and the extent of mixing is very weak for all three stages. This poor transport behaviour of fluid at the bottom of the vessel highlights the likelihood of slow digestion of any food components that are either initially present or which settles there due to density differences.

6. Discussion

6.1. Hydrodynamics of stirred systems

Helical screw shaped impellers are commonly used for mixing and

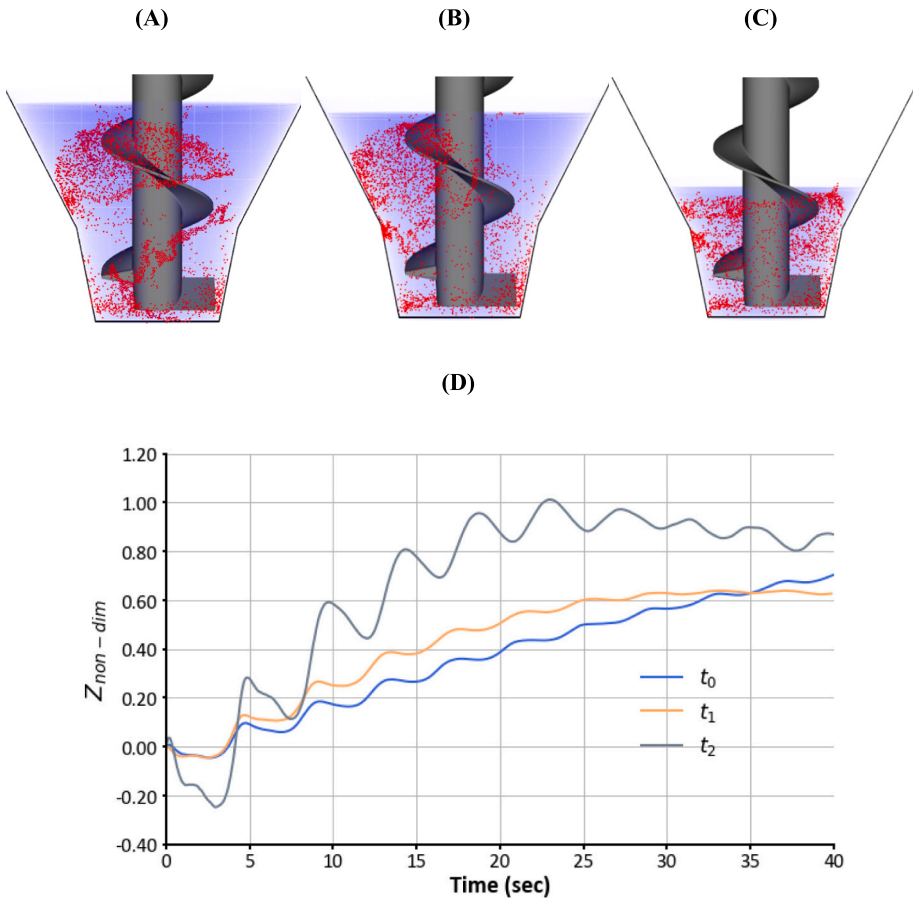

Fig. 9. Side view of the spatial dispersion of SGF injected into the lower corner of the vessel (region ROI1) (coloured red) at 40 s after the start of each gastric stage (A) t_0, (B) t_1 and (C) t_2. (D) Axial dispersion of the SGF as represented by the normalised axial centroid ($Z_{non\text{-}dim}$) for each gastric stage. (For interpretation of the references to colour in this figure legend, the reader is referred to the web version of this article.)

conveying applications in various industries and applications such as tower mills for mineral processing (Sinnott et al., 2011), twin screw extruders for food manufacturing (Robinson & Cleary, 2019; Tagliavini et al., 2018), as well as stirred bioreactor tanks (Amiraftabi et al., 2021). The screw geometry has good transport properties over a broad rheological range from fluids to slurries to dry granular solids and generates strong axial pumping motion along the direction of the impeller shaft. In a vertical configuration, the combination of upward flow within the screw flight and gravitationally driven downflow outside typically creates a bulk axial circulation and a characteristic annular shear zone between the edge of the impeller and the walls of a tank. CFD simulations of screw impellers in cylindrical vessels confirm that high velocity magnitudes are concentrated near the blade tips (Ameur et al., 2016; Aubin et al., 2000) consistent with our model predictions. At higher fluid viscosities, flow becomes increasingly localised around the screw flight and the annular shear zone between impeller and vessel wall becomes less intense for a given screw speed. Ryma et al. (2013) observed a similar trend of increased flow localisation with viscosity in simulations using a Rustom turbine with six blades. Unlike the extensively studied cylindrical vessels, hydrodynamics in conical vessels is less well understood. To date, there are no published CFD studies of the fluid dynamics around the INFOGEST stirrer. This together with prediction of circulation in the V-form titration vessel is the focus of this study.

A known performance issue for screw impellers is their limited ability to generate sufficient shear radially out to the confining wall for large diameter tanks (Ameur et al., 2018). This issue is reflected in our findings, where the upper portion of the conical vessel shows poor mixing for high fill levels in the t_0 and t_1 simulations. Secondary radial and axial circulation structures referred to as "self-feeding zones" arise near the impeller edges in CFD studies of similar stirred tanks (Aubin et al., 2000). When mixing non-Newtonian fluids, these structures can become more prominent and are a characteristic measure of inefficient circulation since they diminish the bulk axial circulation along the screw. Further, poor mixing frequently occurs in narrow clearance gaps between the impeller base and the floor (Leng et al., 2008), consistent with our measurements above. This emphasises the sensitivity of screw impeller performance to vessel geometry and fluid viscosity. Ribbon impellers are more commonly employed in stirred bioreactors. Their outer radial helical ribbon geometry allows for smaller wall clearances and directs axial circulation through the central region (Robinson & Cleary, 2012) when appropriately sized and positioned with respect to vessel geometry (Ameur et al., 2013). Modification of impeller geometry to suit a given vessel can improve mixing performance. For example, Ameur et al. (2018) have demonstrated that conforming impeller blade tip geometry to the shape of a conically curved bottom of the vessel improves mixing quality in this region.

6.2. *Hydrodynamics, enzyme diffusion and reaction kinetics*

Gastric digestion *in vivo* is complex and involves physical breakdown *via* phasic muscular contractions and chemical breakdown which is dependent on sufficient and timely mixing of acid and enzyme secretions with the food meal. Antral waves commence from the middle of the stomach body and mix and propel digesta towards the pylorus. Retropulsive jets from terminal antral contractions near the pylorus transport the digesta back upward creating a bulk antral re-circulation that is fundamental to mixing in the rest of the gastric volume (Pal et al., 2004). The jets also aid mixing, grinding and dissolution of food

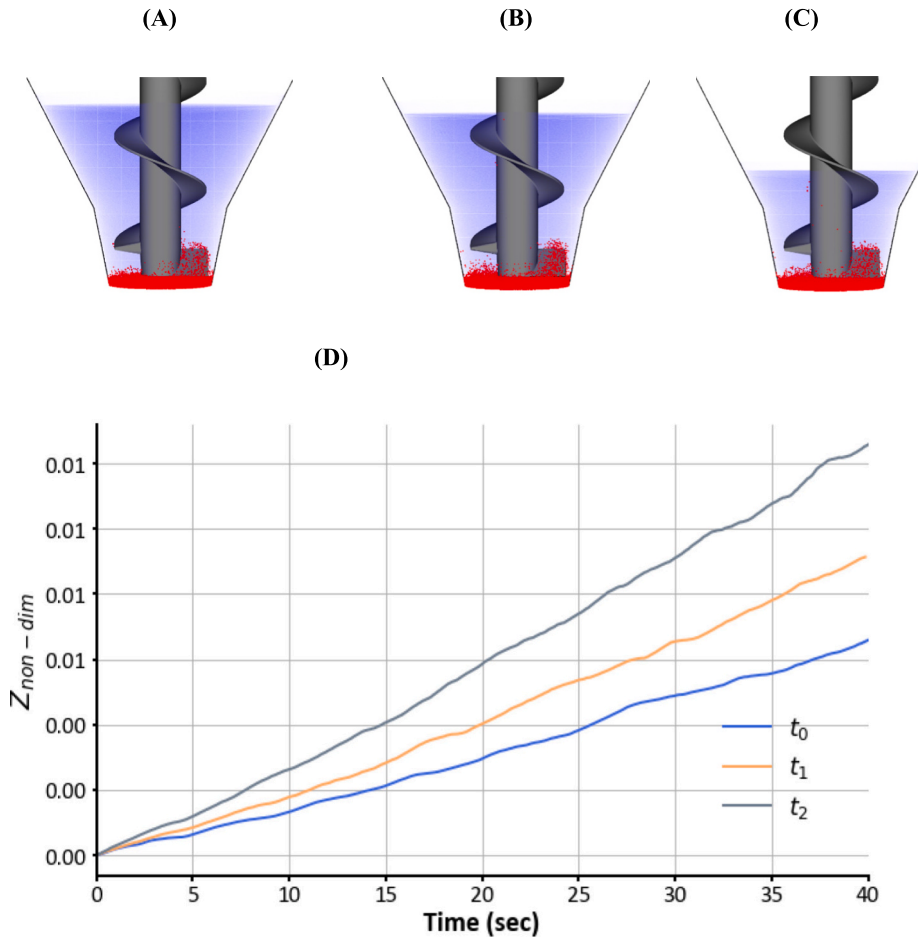

Fig. 10. Side view showing the spatial dispersion (at 40 s) of the small volume of fluid initially located in the basal region under the stirrer (region ROI_2) for gastric stages (A) t_0, (B) t_1 and (C) t_2. (D) Axial dispersion of the initial basal region fluid for each gastric stage represented by its normalised axial centroid $Z_{non\text{-}dim}$.

(Kuhar et al., 2022). The recirculation does not extend fully into the proximal stomach and therefore mixing of digesta in the fundus is much weaker. Well controlled advective-diffusive mixing is important for ensuring sufficient concentrations of enzymes and acid to maintain effective reaction kinetics for protein and lipid hydrolysis.

The hydrodynamic environment of the INFOGEST *in vitro* experiment considered in this paper has some notable differences from the *in vivo* gastric system. The rotating screw impeller creates strong, steady swirling azimuthal flow (Fig. 4, row 3) that weakens with radial distance from the impeller. This behaviour is not present *in vivo*. The shape of the conical vessel and the weaker flow at large radius higher in the vessel intends to mimic the weaker mixing in the gastric fundus. As discussed in the previous section, screw impellers in large radius vessels are often unable to generate sufficient shear out to the vessel wall to prevent stagnation of the flow at the wall with this becoming worse with height in a conical vessel (as shown by shear rate in Fig. 7) and with increasing digesta viscosity (as shown by the change in flow between t_0 and t_1 in Fig. 4, row 3). For an impeller speed of 15 rpm, our model predicts a large annular unmixed region in the upper outer parts of the conical vessel containing around half of the digesta volume in the initial t_0 stage. The motion of the screw generates downward axial propulsion intended to represent phasic peristaltic wall movements to produce a bulk antral recirculation within the vessel, although the location of the driving surfaces is radially inverted so that it is now at the centre of the vessel. However, the high digesta pressures which drive the strong retro-propulsive jets *in vivo* due to terminal antral contraction waves converging on the pylorus cannot easily be represented in this *in vitro* system. This may therefore underpredict the real rate of mixing, grinding and dissolution for more complex foods compared to the low viscosity liquid meal considered here. Our *in silico* results (Fig. 3) do highlight secondary radial/axial recirculation zones at the tips of the screw blade which correspond with regions of moderate shear rate (Fig. 7) and are analogous to local flow structure predicted around *in vivo* contractions (Pal et al., 2004).

The small gap between the base of the impeller and the floor creates a second small unmixed region where food substrate may become trapped and remain undigested. Enzymes and acid are injected into a small local region at the bottom of the vessel. They therefore require significant axial dispersion compared to the *in vivo* environment where secretion occurs over 80 % of the area of the upper stomach body. There, enzyme concentration is more uniform along the wall having a steady radial gradient with distance into the lumen.

Although a detailed analysis of the coupling between transport and reaction kinetics lies beyond the scope of this study, a brief discussion is provided to offer context. As enzymes catalyse reactions, they locally deplete substrate concentrations (Srividhya & Schnell, 2006), generating spatial gradients when introduced into a compact region, such as in the semi-dynamic *in vitro* model. These gradients influence both the catalytic activity of enzymes and their diffusion. In accordance with Michaelis–Menten kinetics, enzymes in regions of high substrate concentration operate close to their maximum reaction rate, V_{max} (Giunta, 2020), whereas in areas of low substrate concentration, they function below V_{max}, leading to reduced reaction rates. In regions near the stirrer edge, the modelled enzyme exhibits a coherent structure of high concentration during the early stage of digestion. Within this structure, when local enzyme concentrations exceed those of the local substrate

concentration, the enzymes cannot function at full catalytic capacity due to limited substrate availability. This may lead to a reduction in the local reaction rate, rendering these areas reaction-limited (Schnell & Maini, 2000). Enzymes diffuse more readily as a function of local substrate concentration and therefore undergo chemotaxis, being preferentially directed to high concentration regions (Mohajerani et al., 2018). Catalytic activity can reduce local viscosity (Hirose & Sugano, 2024) influencing advective transport. Spatial heterogeneity of enzyme distribution can therefore influence both diffusion and advection characteristics, forming a non-linear feedback mechanism. This means the digestion process evolves dynamically, with the rate and extent of reaction influenced by changing local conditions and has the potential to produce a similar extent of spatially heterogeneous flow and hydrolysis as seen *in vivo*.

Restricted transport of enzymes into poorly mixed or stagnant regions reduces enzyme availability and will significantly diminish digestion reaction kinetics in such regions (Robinson, 2015). This will then poorly reflect the behaviour of the *in vivo* system. Notably, the area beneath the stirrer remains stagnant throughout the full gastric cycle (as shown by shear rate in Fig. 7). Based on 1D Fickian diffusion we can define the enzyme diffusion mean free path $x = \sqrt{2Dt}$, where t is time (s) (Mukherjee & Chakravorti, 2015). Pepsin has a diffusivity of D $\approx 1.0 \times 10^{-6}$ cm^2/s (Rakhshi, 2019) and lipase has a diffusivity of D $\approx 3.5 \times 10^{-10}$ cm^2/s in water (Bohr et al., 2019). Over the full 2-h duration of the INFOGEST gastric cycle for our model liquid food, pepsin and lipase will therefore travel an average distance of approximately 1.2 mm and 0.022 mm respectively *via* diffusion alone which is negligible compared to the scale of the vessel. Therefore, advective transport is essential for digestion. In low-flow zones of the INFOGEST mixer, for which the flow speed (u) is <0.5 mm/s, the Péclet number ($Pe = uL/D$) is in the range 10,000–50,000 based on a characteristic length (L) of 10 mm from the stirrer radius. This confirms that the diffusion timescale for pepsin is sufficiently slow that even the very weak advection found into the slow flow regions still dominate enzyme transport. Consequently, in the absence of sufficiently representative advective mixing we may expect restricted digestion kinetics that do not match those of the *in vivo* system.

Digesta viscosity slows advective mixing and can alter the structure of the *in vitro* flow field. Dispersion of introduced enzymes and acid is also affected by viscosity. The radial dispersion rate is 3.2× faster while the axial dispersion is 44 % faster for a 7.1× reduction in viscosity from t_0 to t_2. This demonstrates that digesta viscosity is an important control for how quickly and how completely the added enzymes and acid disperse within the titration vessel. Consequently, digestion of higher viscosity content in higher fill volumes in the early gastric stages may be slowed by the presence of unmixed regions hindering digestion and nutrient bioaccessibility as intended in the semi-dynamic protocol.

7. Conclusion

An SPH model has been presented for simulating stirring of a Newtonian liquid food at three stages of the gastric phase of an *in vitro* model following the standardised INFOGEST semi-dynamic protocols. The *in silico* model takes into account changes in viscosity and fill volume that occur between the gastric stages. The rotating stirrer imparts a complex three-dimensional swirling flow to the fluid with differing amounts of radial, tangential and axial transport. The tangential swirling flow is local to the region immediately around the stirrer while the paddle at the base of the stirrer imparts an upward axial motion to the fluid generating axial recirculation. Strong radial recirculation around the outer radial edge of the helical blade creates high peak shear rates. Transport characteristics of the flow change between gastric stages due to changes in digesta viscosity and fluid fill level. During earlier stage digestion when viscosity and fluid volume are higher, the flow remains localised to the stirrer while fluid near the vessel wall moves only slowly. Comparison of advection and diffusion timescales for this stirrer indicate that this could have potential implications in slowing digestion and adversely impacting measured digestion kinetics and bioaccessibility predictions.

Higher digesta viscosity is found to impede radial dispersion of fluid, which could result in reduced enzyme and acid availability and potentially slow early-stage digestion in some parts of the fluid. Furthermore, stagnant regions observed in the early digestion stages and located in the upper regions near the free surface and adjacent to vessel wall may contribute to undigested food or delays in digestion initiation. The presence of an unmixed region beneath the stirrer suggests that any denser material or segregated solids (for INFOGEST models with more complex foods) settling to the bottom of the vessel may undergo incomplete digestion. The model predictions for the hydrodynamics and mixing performance of the INFOGEST stirrer provide encouraging evidence that it is able to produce a similar extent of spatially inhomogeneous flow and hydrolysis as exists *in vivo*. As such, the stirrer appears well suited for application in semi-dynamic gastric protocols for low viscosity liquid foods.

The results of this study further suggest some potential design changes for the semi-dynamic protocol gastric phase that could be considered to help fine-tune stirrer performance:

- The size of the unmixed digesta volume may be modified by reducing clearances between wall and blade (either by selection of a narrower flask or increasing the screw blade diameter) so that the swirling flow can extend fully out to the walls to increase mobility of more of the digesta volume.
- Alternatively, the size of the unmixed regions can also be controlled by judicious choice of appropriate stirrer speed to both accommodate changes in fluid viscosity throughout the digestion process and maintain consistent mixing performance that represents *in vivo* antral circulation.
- Repositioning of the feed tubes for better dispersion of added enzyme/acid/SGF particularly for high viscosity digesta in the early gastric stages, and
- Reduced clearance between bottom of the stirrer and the floor, or potential redesign of the stirrer geometry to better mobilise fluid below the current stirrer.

This first detailed flow analysis of the gastric phase of a semi-dynamic *in vitro* model (using an INFOGEST overhead stirrer) provides a powerful *in silico* approach which can easily be used as a virtual prototyping design tool. It has the potential to support extension of the INFOGEST semi-dynamic protocol to include new guidelines for optimal agitation control across a broad range of food materials and digesta rheology. This may also incorporate more detailed or even adaptive control strategies to respond to rapid rheological changes during digestion emulating real physiological behaviour. Finally, characterisation of the *in vivo* gastric environment through simulation can yield essential data about physiological conditions (*e.g.* shear rates) that can be used to build more realistic *in vitro* models.

Future work will take greater advantage of the Lagrangian SPH methodology to investigate *in vitro* mixing for more complex, multiphase food materials (including non-Newtonian rheology over a broader viscosity range) over a range of stirrer speeds. We will also seek to extend existing *in silico* gastric models to simulate the *in vivo* environment and determine physiologically relevant hydrodynamic data (including shear rates, motility and mixing) which are necessary to inform next generation *in vitro* model designs.

CRediT authorship contribution statement

Shaktivesh Shaktivesh: Visualization, Formal analysis, Writing – original draft, Investigation. **Matt D. Sinnott:** Writing – original draft, Project administration, Conceptualization, Writing – review & editing, Supervision, Formal analysis. **Alan R. Mackie:** Writing – review & editing, Conceptualization, Investigation. **Paul W. Cleary:** Software,

Methodology, Writing – review & editing, Resources, Formal analysis.

Declaration of competing interest

The authors declare that they have no known competing financial interests or personal relationships that could have appeared to influence the work reported in this paper.

Acknowledgements

This study is fully funded by the CSIRO Microbiome for One System Health (MOSH) Future Science Platform (FSP) (research.csiro.au/microbiome/).

Data availability

Data will be made available on request.

References

Alminger, M., Aura, A. M., Bohn, T., Dufour, C., El, S. N., Gomes, A., … Santos, C. N. (2014). In vitro models for studying secondary plant metabolite digestion and bioaccessibility. *Comprehensive Reviews in Food Science and Food Safety, 13*(4), 413–436. https://doi.org/10.1111/1541-4337.12081

Ameur, H., Bouzit, M., & Ghenaim, A. (2013). Hydrodynamics in a vessel stirred by simple and double helical ribbon impellers. *Central European Journal of Engineering, 3*(1), 87–98. https://doi.org/10.2478/S13531-012-0045-X/MACHINEREADABLECITATION/RIS

Ameur, H., Kamla, Y., Hadjeb, A., Arab, I. M., & Sahel, D. (2016). Data on mixing of viscous fluids by helical screw impellers in cylindrical vessels. *Data in Brief, 8*, 220–224. https://doi.org/10.1016/J.DIB.2016.05.036

Ameur, H., Kamla, Y., & Sahel, D. (2018). Performance of helical ribbon and screw impellers for mixing viscous fluids in cylindrical reactors. *ChemEngineering, 2*(2), Article 26. https://doi.org/10.3390/CHEMENGINEERING2020026

Amiraftabi, M., Khiadani, M., Mohammed, H. A., & Arshad, A. (2021). CFD-PBM and experimental investigation of a shear thinning fluid in a gas-liquid tank agitated by a helical ribbon impeller. *Separation and Purification Technology, 272*, Article 118855. https://doi.org/10.1016/J.SEPPUR.2021.118855

Aubin, J., Naude, I., Bertrand, J., & Xuereb, C. (2000). Blending of Newtonian and shear-thinning fluids in a tank stirred with a helical screw agitator. *Chemical Engineering Research and Design, 78*(8), 1105–1114. https://doi.org/10.1205/026387600528382

Bohr, S. S. R., Lund, P. M., Kallenbach, A. S., Pinholt, H., Thomsen, J., Iversen, L., & Hatzakis, N. S. (2019). Direct observation of Thermomyces lanuginosus lipase diffusional states by single particle tracking and their remodeling by mutations and inhibition. *Scientific Reports, 9*(1), 16169.

Bornhorst, G. M. (2017). Gastric mixing during food digestion: Mechanisms and applications. *Annual Review of Food Science and Technology, 8*, 523–542. https://doi.org/10.1146/ANNUREV-FOOD-030216-025802/CITE/REFWORKS

Brodkorb, A., Egger, L., Alminger, M., Alvito, P., Assunção, R., Ballance, S., Bohn, T., Bourlieu-Lacanal, C., Boutrou, R., Carrière, F., Clemente, A., Corredig, M., Dupont, D., Dufour, C., Edwards, C., Golding, M., Karakaya, S., Kirkhus, B., Le Feunteun, S., & Recio, I. (2019). INFOGEST static in vitro simulation of gastrointestinal food digestion. *Nature Protocols, 14*(4), 991–1014. https://doi.org/10.1038/S41596-018-0119-1

Cardoso, C., Afonso, C., Lourenço, H., Costa, S., & Nunes, M. L. (2015). Bioaccessibility assessment methodologies and their consequences for the risk–benefit evaluation of food. *Trends in Food Science & Technology, 41*(1), 5–23. https://doi.org/10.1016/J.TIFS.2014.08.008

Cleary, P., Ha, J., Alguine, V., & Nguyen, T. (2002). Flow modelling in casting processes. *Applied Mathematical Modelling, 26*(2), 171–190. https://doi.org/10.1016/S0307-904X(01)00054-3

Cleary, P. W., Harrison, S. M., Sinnott, M. D., Pereira, G. G., Prakash, M., Cohen, R. C. Z., … Stokes, N. (2021). Application of SPH to single and multiphase geophysical, biophysical and industrial fluid flows. *International Journal of Computational Fluid Dynamics, 35*, 22–78. https://doi.org/10.1080/10618562.2020.1841897

Cleary, P. W., Prakash, M., Ha, J., Stokes, N., & Scott, C. (2007). Smooth particle hydrodynamics: Status and future potential. *Progress in Computational Fluid Dynamics, 7*(2–4), 70–90. https://doi.org/10.1504/pcfd.2007.013000

Cleary, P. W., Savage, G., Ha, J., & Prakash, M. (2014). Flow analysis and validation of numerical modelling for a thin walled high pressure die casting using SPH. *Computational Particle Mechanics, 1*(3), 229–243. https://doi.org/10.1007/S40571-014-0025-4/FIGURES/5

Cleary, P. W., Thomas, D., Hetherton, L., Bolger, M., Hilton, J. E., & Watkins, D. (2020). Workspace: A workflow platform for supporting development and deployment of modelling and simulation. *Mathematics and Computers in Simulation, 175*, 25–61. https://doi.org/10.1016/J.MATCOM.2019.11.011

Cummins, S. J., Silvester, T. B., & Cleary, P. W. (2012). Three-dimensional wave impact on a rigid structure using smoothed particle hydrodynamics. *International Journal for Numerical Methods in Fluids, 68*(12), 1471–1496. https://doi.org/10.1002/FLD.2539

Ferrua, M. J., Xue, Z., & Singh, R. P. (2014). Dynamics of gastric contents during digestion—Computational and rheological considerations. *Food Structures, Digestion and Health, 319–360*. https://doi.org/10.1016/B978-0-12-404610-8.00012-8

Giunta, G. (2020). *Spatio-temporal organization of enzymatic reactions*. Fakultät für Physik. PhD Thesis.

Harrison, S. M., Cleary, P. W., & Sinnott, M. D. (2018). Investigating mixing and emptying for aqueous liquid content from the stomach using a coupled biomechanical-SPH model. *Food & Function, 9*(6), 3202–3219. https://doi.org/10.1039/c7fo01226h

Hirose, R., & Sugano, K. (2024). Effect of food viscosity on drug dissolution. *Pharmaceutical Research, 41*(1), 105–112. https://doi.org/10.1007/S11095-023-03620-Y/METRICS

Jin, Y., Wilde, P. J., Li, C., Jin, W., Han, J., & Liu, W. (2023). Impact of food viscosity on in vitro gastric emptying using dynamic and semi-dynamic models. *Food Hydrocolloids, 137*, Article 108410. https://doi.org/10.1016/J.FOODHYD.2022.108410

Kuhar, S., Lee, J. H., Seo, J. H., Pasricha, P. J., & Mittal, R. (2022). Effect of stomach motility on food hydrolysis and gastric emptying: Insight from computational models. *Physics of Fluids, 34*(11).

Leng, D. E., Katti, S. S., & Atiemo-Obeng, V. (2008). Industrial mixing technology. In *Albright's chemical engineering handbook* (pp. 631–724). CRC Press. https://doi.org/10.1201/9781420014389-13.

Li, C., & Jin, Y. (2023). Digestion of meat proteins in a human-stomach: A CFD simulation study. *Innovative Food Science & Emerging Technologies, 83*, Article 103252. https://doi.org/10.1016/J.IFSET.2022.103252

Li, Y., & Kong, F. (2022). Simulating human gastrointestinal motility in dynamic in vitro models. *Comprehensive Reviews in Food Science and Food Safety, 21*(5), 3804–3833.

Liu, X., Harrison, S. M., Fletcher, D. F., & Cleary, P. W. (2023). Numerical simulation of buoyancy–driven flow in a human stomach geometry: Comparison of SPH and FVM models. *Applied Mathematical Modelling, 124*, 367–392. https://doi.org/10.1016/J.APM.2023.08.004

Logan, K., Wright, A. J., & Douglas Goff, H. (2014). Correlating the structure and in vitro digestion viscosities of different pectin fibers to in vivo human satiety. *Food & Function, 6*, 63. https://doi.org/10.1039/c4fo00543k

Lucas-González, R., Viuda-Martos, M., Pérez-Alvarez, J. A., & Fernández-López, J. (2018). In vitro digestion models suitable for foods: Opportunities for new fields of application and challenges. *Food Research International, 107*, 423–436. https://doi.org/10.1016/J.FOODRES.2018.02.055

Mohajerani, F., Zhao, X., Somasundar, A., Velegol, D., & Sen, A. (2018). A theory of enzyme chemotaxis: From experiments to modeling. *Biochemistry, 57*(43), 6256–6263. https://doi.org/10.1021/acs.biochem.8b00801

Monaghan, J. J. (2005). Smoothed particle hydrodynamics. *Reports on Progress in Physics, 68*(8), 1703–1759. https://doi.org/10.1088/0034-4885/68/8/R01

Mukherjee, M., & Chakravorti, S. (2015). Assessment of moisture diffusion distance in pressboard insulation within transformer using Fick's law. In *2014 18th National Power Systems Conference, NPSC 2014*. https://doi.org/10.1109/NPSC.2014.7103795

Mulet-Cabero, A. I., Egger, L., Portmann, R., Ménard, O., Marze, S., Minekus, M., … Mackie, A. (2020). A standardised semi-dynamic in vitro digestion method suitable for food – An international consensus. *Food & Function, 11*(2), 1702–1720. https://doi.org/10.1039/C9FO01293A

Pal, A., Indireshkumar, K., Schwizer, W., Abrahamsson, B., Fried, M., & Brasseur, J. G. (2004). Gastric flow and mixing studied using computer simulation. *Proceedings of the Royal Society of London. Series B: Biological Sciences, 271*(1557), 2587–2594.

Prakash, M., Cleary, P. W., Ha, J., Noui-Mehidi, M. N., Blackburn, H. M., & Brooks, G. (2007). Simulation of suspension of solids in a liquid in a mixing tank using SPH and comparison with physical modelling experiments. *Progress in Computational Fluid Dynamics, 7*(2–4), 91–100. https://doi.org/10.1504/PCFD.2007.013001

Rakhshi, E. (2019). *Exploration of pepsin diffusion in solid food particles by dynamic fluorescence techniques*. https://doi.org/10.34894/VQ1DJA

Robinson, M., & Cleary, P. W. (2012). Flow and mixing performance in helical ribbon mixers. *Chemical Engineering Science, 84*, 382–398. https://doi.org/10.1016/J.CES.2012.08.044

Robinson, M., & Cleary, P. W. (2019). Effect of geometry and fill level on the transport and mixing behaviour of a co-rotating twin screw extruder. *Computational Particle Mechanics, 6*(2), 227–247. https://doi.org/10.1007/S40571-018-0210-Y

Robinson, P. K. (2015). Enzymes: Principles and biotechnological applications. *Essays in Biochemistry, 59*, 1. https://doi.org/10.1042/BSE0590001

Ryma, A., Dhaouadi, H., Mhiri, H., & Bournot, P. (2013). CFD study of the fluid viscosity variation and effect on the flow in a stirred tank. *World Academy of Science, Engineering and Technology, International Journal of Mechanical, Aerospace, Industrial, Mechatronic and Manufacturing Engineering, 7*(3), 470–478.

Schnell, S., & Maini, P. K. (2000). Enzyme kinetics at high enzyme concentration. *Bulletin of Mathematical Biology, 62*(3), 483–499. https://doi.org/10.1006/BULM.1999.0163/METRICS

Sinnott, M., Cleary, P. W., & Morrison, R. D. (2011). Slurry flow in a tower mill. *Minerals Engineering, 24*(2), 152–159. https://doi.org/10.1016/J.MINENG.2010.11.002

Sinnott, M. D., Harrison, S. M., & Cleary, P. W. (2021). A particle-based modelling approach to food processing operations. *Food and Bioproducts Processing, 127*, 14–57.

Srividhya, J., & Schnell, S. (2006). Why substrate depletion has apparent first-order kinetics in enzymatic digestion. *Computational Biology and Chemistry, 30*(3), 209–214. https://doi.org/10.1016/J.COMPBIOLCHEM.2006.03.003

Tagliavini, G., Solari, F., & Montanari, R. (2018). CFD simulation of a co-rotating twin-screw extruder: Validation of a rheological model for a starch-based dough for snack food. *International Journal of Food Engineering, 14*(2). https://doi.org/10.1515/IJFE-2017-0116/MACHINEREADABLECITATION/RIS

Workspace – A powerful scientific workflow framework, (n.d.). https://research.csiro.au/workspace/ (accessed October 4, 2024).